

THE PROCESSING OF ScaRaB DATA

M. Viollier, C. Standfuss
LMD/CNRS Ecole Polytechnique
91128 Palaiseau Cedex, France

Megha-Tropiques: 1st International Workshop, Bangalore, 1999

1 Introduction

Instantaneous radiances measured by ScaRaB (see Viollier et al, this issue) concern only one space direction: the satellite-to-target direction. From this unique measurement, we have to estimate the radiances in all the upward directions (angular extrapolation) in order to compute fluxes. Flux estimates have then to be sorted and averaged on a standard geographic grid (instantaneous regional means). Each region is observed with limited time coverage. A region is sampled, at most, twice a day by one polar satellite. Diurnal modelling of flux variation is necessary to get daily and monthly means. The ScaRaB data processing indeed has to perform at least a threefold (observation angle, region and time) interpolation and integration algorithm. In order to minimise biases between the ERBE and ScaRaB time series, the first version of the ScaRaB data processing has been developed as an "ERBE-like version".

The ERBE-like version of data processing is based on algorithms according to Smith *et al.* (1986), Wielicki and Green (1989), and Suttles *et al.* (1988a, 1988b) for inversion, Brooks *et al.* (1986) for the Monthly Time Space Averaging. Additionally, the spectral corrections had to be studied to fit the ScaRaB characteristics (Viollier et al., 1995). The ERBE-like version has made the data processing between ERBE, ScaRaB and CERES homogeneous. It is summarised in section 2.

New advanced algorithms concerning LW and SW angular corrections are described in section 3

It is difficult to provide a complete error analysis of the ERB determination due to the impact of both, instrument uncertainties and limited performance of the extrapolation algorithms. Errors at different scales are discussed in section 4.

Finally, the tropical monthly means are simulated for the ScaRaB/Megha-Tropiques mission (section 5).

2 ERBE-Like Algorithms

2.1 Spectral and Angular Corrections

One of the keys to the determination of the Earth Radiation Budget is the "scene identification". It is a major parameter in all steps of the processing: spectral corrections, radiance-to-flux conversion, time-space averaging, and cloud radiative forcing calculation. In order to minimise biases between ERBE and ScaRaB time series, the same 12 scene classifications as ERBE (Smith *et al.* 1986) are used, based on the combination of five geotypes (ocean, land, snow-ice, desert, coast) and four cloud categories (clear, partly cloudy, mostly cloudy, overcast). The algorithm of scene identification is the Maximum Likelihood Estimation (MLE: Wielicki and Green 1989) which compares the measured LW and SW radiances to a predefined set of radiances for the appropriate geometry of view and the geographic zone. The algorithm is adjusted to account for regional variations of clear-sky surface albedos and for diurnal as well as for regional variations of LW fluxes of land and desert geotypes. During the night, the LW radiance is used for MLE with 1D computation. During the daytime, both LW and SW radiances allow a 2D computation.

Once the scene identified, the raw radiances are first corrected for spectral filtering. The ScaRaB spectral response is not perfectly flat, and diminishes substantially at wavelengths below 0.4 μm . Using the simulation of reflected SW radiances for 530 cases, Viollier *et al.* (1995) find that, for clear and partly cloudy ocean scenes, a correction of +5% significantly reduces the spectral filtering errors (standard deviation 1.2 Wm^{-2} for the 530 cases). Although one might expect a smaller nonzero correction for mostly cloudy ocean scenes, this was not confirmed by the calculation, and no correction is applied. Clear and partly cloudy ocean scenes appear blue from space, but the white reflection of clouds overwhelms the blue in a mostly cloudy scene.

The second correction based on the scene identification is the angular correction, more precisely the use of an anisotropic factor for radiance-to-flux conversion. The ERBE angular models (Suttles *et al.* 1988, a,b) have been used to ensure consistency between ERBE and ScaRaB products. It should be remembered that SW angular corrections may be greater than a factor 4 and are the major source of uncertainty for instantaneous and daily mean SW flux estimates.

The results of the computations are stored in the A2 file (table 1)

<p>Table 1:A2 File Each record contains 48 seconds of data (8 scan cycles of 51 elementary measurements) in the following form</p> <p>Julian date at the beginning of the record. Satellite and Sun locations relative to the Earth' centre at the beginning and end of record.</p> <p>Then for each of the 408 Earth observations:</p> <ul style="list-style-type: none"> - location (colatitude et longitude) - filtered radiances (T, SW, Vis, Ir) - view geometry (θ_{sun}, θ_{view}, ϕ) - unfiltered radiances (SW, LW) - flux estimate at the top of the atmosphere (SW, LW) - scene identification : geotype et cloud category

2.2 Space and Time Averaging

The above mentioned steps of the processing were done at the “ pixel ” level. The remaining computations deal with spatial averages of the elementary observations over geographical areas of $2.5^\circ \times 2.5^\circ$ in latitude and longitude. These averages, called instantaneous regional means, are collected for an entire month and region by region. They are stored in the A3-MRI files (table 2).

<p>Table 2: A3-MRI File Each record contains successive instantaneous regional means per region for one month with:</p> <ul style="list-style-type: none"> - region index (between 1 et 10368) - monthly hour bin (between 1 et 31 x 24) - day and averaged time (TU) of the observation - averaged view geometry (θ_{sun}, θ_{view}, ϕ) - solar irradiance (W.m^{-2}) - fluxes SW and LW (Wm^{-2}), means of observations for the 4 cloud covers and statistics (min, max, standard deviation and number of elementary observations)

Time sampling is another important issue for ERB determination. Indeed, except at high latitude, a satellite in a near polar orbit observes a particular region only twice a day. Two observations (one in the SW) are not sufficient to account for the diurnal variations of the Earth surface-atmosphere system, which are related to variations of temperature and cloudiness driven by the daily cycle of insolation. In the SW domain the instantaneous regional means are interpolated or extrapolated in local time for the entire day (figures 1a,b, c) using the same algorithms as ERBE (Brooks *et al.* 1986). They can be summarised in what follows. Hereafter, time values are expressed in local mean time or local solar time (LST). The aim of the algorithms is to extrapolate flux from observation time t_{obs} to the 24 local hour boxes centred on the half local hours t_h : 0030, 0130,..., 2330. First, we assume we have only one SW observation per day at t_{obs} (figure 1a). From the albedo (α) definition, we write the shortwave reflected flux $M_{\text{sw}}(t)$ at time t

$$M_{\text{sw}}(t) = E_o(d) \cos(\theta_o(t))\alpha(t)$$

where $E_o(d)$ is the solar constant for the day d and θ_o is the solar zenith angle.

Since the variations of $E_o(d)$ are negligible during the day, the basic time-extrapolation then is

$$M_{sw}(t_h) = \frac{\cos(\theta_o(t_h)) \alpha(t_h)}{\cos(\theta_o(t_{obs})) \alpha(t_{obs})} M_{sw}(t_{obs}) \quad 2$$

showing that the first source of variation is the cosine insolation term. The time variations of albedo may be due to changes in meteorology or in solar zenith angle. Except over clear scenes without relief or specular reflection like snow and some deserts, the albedo strongly increases with θ_o . The worst case is the ocean: albedo increases from 0.07 to 0.30 (a factor 4) when the solar zenith angle varies from 0 to 85°. For clouds, the albedo increases typically from 0.42 to 0.65. To take into account these variations, the directional albedo function δ has been introduced depending on the scene type i and normalised by reference to the albedo value at overhead sun A ($\theta_o=0$)

$$\alpha_i(\theta_o) = A_i \delta_i(\theta_o) \quad 3$$

Over extended regions, the albedo is a contribution of different scene types i . Then equation 2 becomes

$$M_{sw}(t_h) = \frac{\cos(\theta_o(t_h)) \sum_i f_i(t_h) A_i \delta_i(\theta_o(t_h))}{\cos(\theta_o(t_{obs})) \sum_i f_i(t_{obs}) A_i \delta_i(\theta_o(t_{obs}))} M_{sw}(t_{obs}) \quad 4$$

f_i is the fraction of the different scene types within the region. The ERBE algorithm is based on the 12 scene types defined by Suttles et al. (1988a). In the ERBE processing all the parameters of equation 4 are available, except $f_i(t_h)$. The ERBE algorithm assumes $f_i(t_h) = f_i(t_{obs})$, meaning that it takes no account for any diurnal change in cloud cover.

When at least 2 SW observations are available at t_{obs1} and t_{obs2} (figures 1b and c) equation 4 provides 2 extrapolated flux estimations: $M_{sw}(t_h, t_{obs1})$ and $M_{sw}(t_h, t_{obs2})$. Between the corresponding $h1$ and $h2$ LST, the flux is interpolated according to

$$M_{sw}(t_h) = \frac{(t_{obs2} - t_h) M_{sw}(t_h, t_{obs1}) + (t_h - t_{obs1}) M_{sw}(t_h, t_{obs2})}{t_{obs2} - t_{obs1}} \quad 5$$

This equation, equivalent to equation 8 of Brooks et al (1986), assumes that the observed scene fractions change linearly with time from $h1$ to $h2$. Equations 4 and 5 are the basic statements of the SW Diurnal Interpolation and Extrapolation Procedure (DIEP).

In the LW domain, the radiant flux interpolation is linear over ocean and snow-ice, but uses a daytime half-sine fit over land/desert and coastal scenes (figure 2) if all daytime fluxes are above the adjacent night-time fluxes. Region by region, the estimated local hourly radiant fluxes are then averaged (integrated for SW) to compute the daily means, the monthly means of the diurnal variation and the overall monthly means.

The results of these computations are stored in the A3-MRMJ file (table 3).

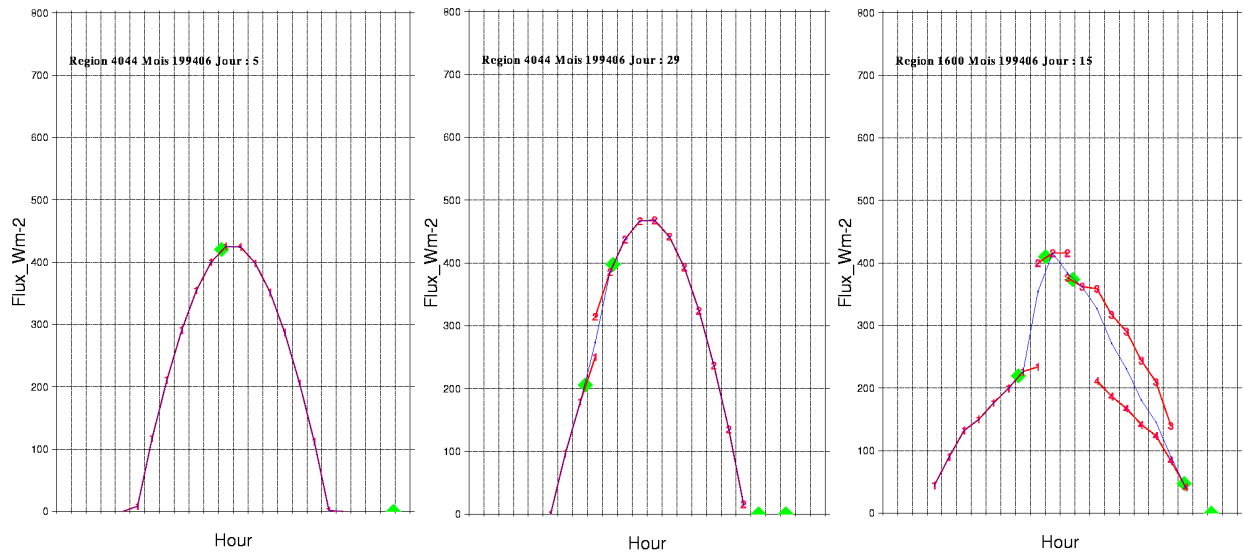


Figure 1 a, b, c: Diurnal Interpolation Extrapolation Procedure in the SW domain: case of one (left), two (middle) and several (right) measurements per days. Grey diamonds correspond to measured fluxes. Numbers 1 to 4 indicate the extrapolated values from the first to the fourth observation respectively (equation 4). The thin line is the interpolation between extrapolated values from adjacent measurements (equation 5).

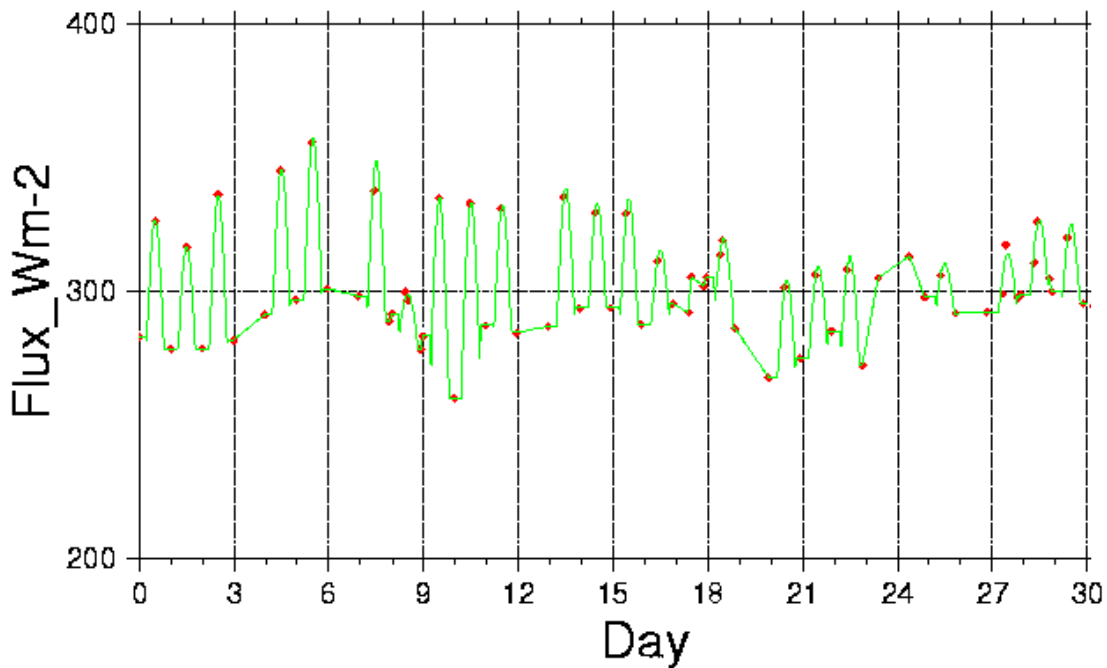


Figure 2: Diurnal Interpolation Extrapolation Procedure in the LW domain (Sahara region, June 1994). Over clear-sky desert regions the condition to apply the half-sinus fit is fulfilled for most days. If not, linear interpolation is applied.

Table 3: A3-MRMJ File

Each record contains monthly properties for one region.:

- region index (between 1 et 10368)
- geotype (ocean, land, ice, desert, coast)
- scene fraction (clear, partly cloudy, mostly cloudy, overcast)
- SW et LW (Wm^{-2}) fluxes and related statistics
- albedo, net flux (Wm^{-2})
- same (SW et LW fluxes, albedo and net flux) but with clear-sky observations

3 Improved algorithms and use of auxiliary channels

Several ways to improve the ERBE-type processing have been studied.

Instead of using the LW anisotropic emission factor tabulated for different viewing zenith angles, seasons, latitude band, and scene type, the angular LW correction is parametrised (Stubenrauch et al, 1993) as a function of the atmospheric pseudo-absorptance defined as the normalised difference between the broadband LW radiance (from ScaRaB channels 3 and 2) and the integrated Planck emission at the 11.5 μm brightness temperature derived from the ScaRaB window channel 4. In a broad sense, the pseudo-absorptance takes into account the greenhouse gas effect.

New SW angular corrections have been computed for desert scenes using Meteosat data (Capderou 1998) and other angular models are under development using POLDER/ADEOS data (Deschamps et al. 1994). The CERES team also is developing new broad-band angular models for an expanded set of scene types, using both existing Nimbus-7/ERB and ERBE data, and expected multi-angular views from the CERES scanner pairs to be flown on the EOS-AM and PM platforms (Wielicki *et al.* 1996). For the diurnal interpolation, Standfuss et al (1998) propose to use a diurnal climatology of the planetary albedo to improve the reflected solar flux monthly means estimates. The regional diurnal (hourly) albedo climatology is derived for each month from the 5-year data record of ERBS. The new method extrapolates the diurnal albedo cycle from each observation concurrently assuming (1) constant cloudiness conditions, i.e. equations 4 and 5 and (2) proportionality to the regional albedo climatology. The choice depends upon the compatibility of the instantaneous observation with the climatological value at observation time: with increasing disagreement between observed and climatological albedo, the use of the climatology for diurnal extrapolation is increasingly restricted.

The two ScaRaB narrow-band radiances are used to refine cloud scenes taking into account cloud phase and spatial heterogeneity (Briand et al., 1997, Briand et al., 1999). This is done by applying the ISCCP algorithms (Rossow et al., 1996) to the ScaRaB narrow-band radiances. General assessment is obtained by comparing ScaRaB data, ScaRaB ISCCP-reprocessed data and real ISCCP data. The real ISCCP data provide larger information since the initial resolution is about 5 km. Analysing the angular behaviour of better characterised scenes should lead to more precise angular corrections.

Auxiliary channels have also been used in several studies dealing with the Narrow band to broad band conversion (Li and Trishchenko, 1999, Doelling et al., 1998, Bouffies et al., 1998, Trishchenko and Li, 1998).

4-Error analysis

Many error types may be accumulated in the different processing steps. The main sources of error are related to the radiance calibration, to the conversion of radiances to fluxes and to the modelling of diurnal variation of fluxes. We focus the discussion on the SW domain for which the errors are the largest.

4--1 Sensitivity of the computations to the SW calibration.

The absolute calibration and in-flight reliability are more difficult to assess in the SW than in the LW domain. According to Kandel et al. (1998), the SW radiance accuracy was 2% for ScaRaB/Meteor, and it is expected to be 1% for Ceres (Wielicki et al., 1996). The propagation of any calibration error through to the monthly averages is not necessary linear. On the contrary the calibration error may amplify or reduce the nominal proportional error, since it acts first to change the cloud identification, and then the spectral, angular and diurnal corrections, all depending on the scene identification.

Figures 3a and b show the impact of calibration errors on the SW instantaneous and monthly mean estimates from simulations using September 1994 ScaRaB data. The simulated calibration difference of 2% affects the cloud cover identification, one of the strong characteristics of anisotropy from which fluxes are computed. The impact on the instantaneous flux ranges from -4 to + 16 W.m^{-2} , the average is 3.9 Wm^{-2} , rms difference is 4.8 Wm^{-2} . For monthly means the errors are reduced, the average is 1.5 Wm^{-2} , rms difference is 1.6 Wm^{-2} .

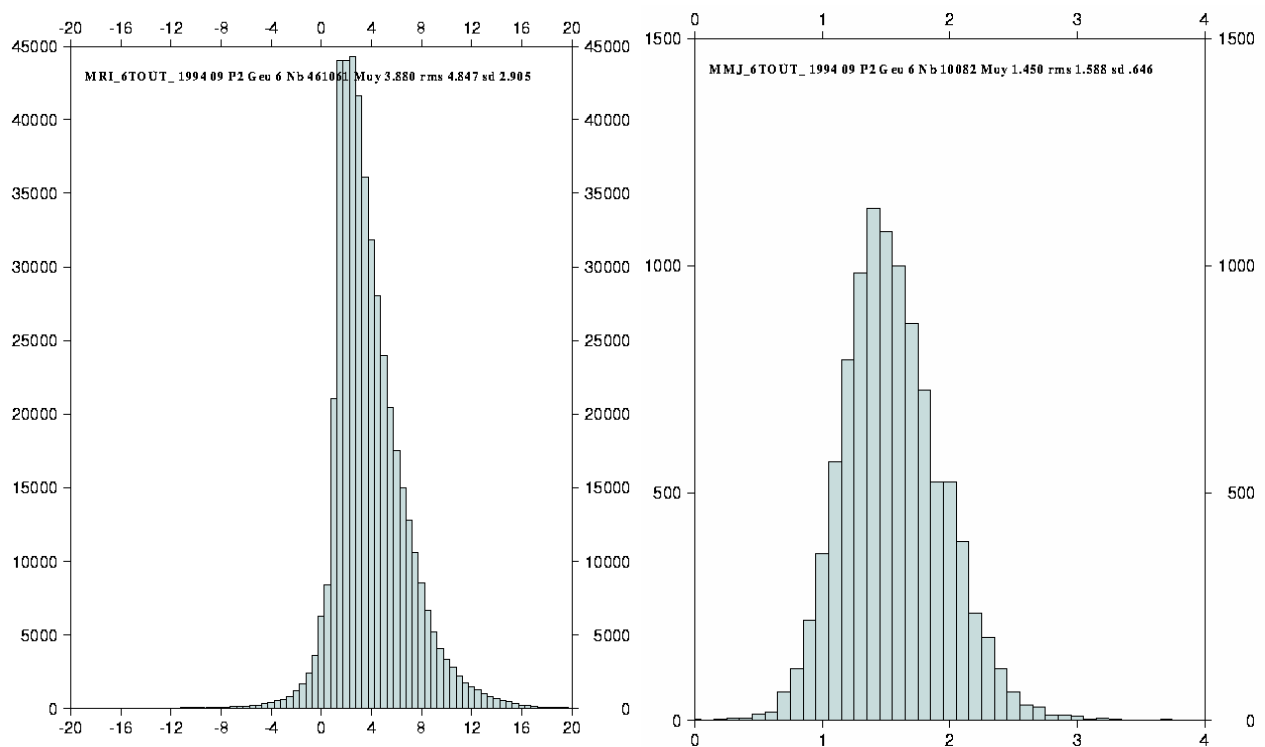


Figure 3a (left) Impact of a simulated 2% calibration error in the SW channel on the computation of the regional instantaneous estimates of the SW reflected flux. The fluxes (X axe of the histogram) are in Wm^{-2} .

Figure 3b (right), same but impact on the monthly means.

4-2 Error on angular correction.

Individual misclassification of scenes can result in erroneous angular corrections (e.g. Ye and Coakley, 1996), and even if the scene classification is correct, angular correction uses a model (in particular a bi-directional reflectance distribution function or BRDF in the SW) which is valid only statistically. By checking the scene identification with concurrent AVHRR scene analysis, Diekmann and Smith (1989) found that the standard deviation of SW errors due to scene misclassification may be as large as 13% of the respective exitances. Extreme errors may occur when a scene is classified partly cloudy and mostly cloudy sky over ocean. By comparing simultaneous instantaneous regional flux estimates from ERBS and NOAA, Dlhopsky et al (1994) found the standard deviation of SW differences of 13% for clear and partly cloudy sky and 9% for mostly cloudy

and overcast sky. There is a tendency for increasing errors with increasing view zenith angle, due to bigger pixel size and geometrical effect (non-observed gaps, shadowing, limb effects).

5 Simulation of diurnal modelling for ERB monthly means of the Megha-Tropiques

Before performing simulations, a reference data set or 'truth' has to be defined. We use the ERBE observations of December 1986, when three satellites (NOAA-9, NOAA-10, ERBS) obtained the highest temporal resolution of ERB satellite observations. Our time-interpolation procedure (section 2.2) is applied to the instantaneous regional means from the 3 satellites, it gives the extrapolated values at all the 744 local hours in the month. These regional hourly values are considered to represent the true diurnal cycles of the reflected SW flux (instantaneous reference data set), as well as the reference monthly means.

In the simulation, orbits are assumed as circular at an altitude of 820 km and an inclination of 20° (figure 4). The instantaneous pixel centres are located assuming the mission instrument a cross-track fixed-azimuth scanner with the ScaRaB characteristics (figure 5). The local time of the observations are then computed (table 4) and the corresponding fictitious instantaneous fluxes (not radiance, the angular corrections are excluded from this simulation) can be extracted from the reference data-set and used in the ERBE-type SW DIEP. The results of this procedure are the simulated monthly means for LW (figure 6) and SW (figure 8) which have to be compared with the corresponding reference or 'truth' monthly means. The differences between Megha-Tropiques simulation and 'truth' are shown on figures 7 and 9, respectively for LW and SW.

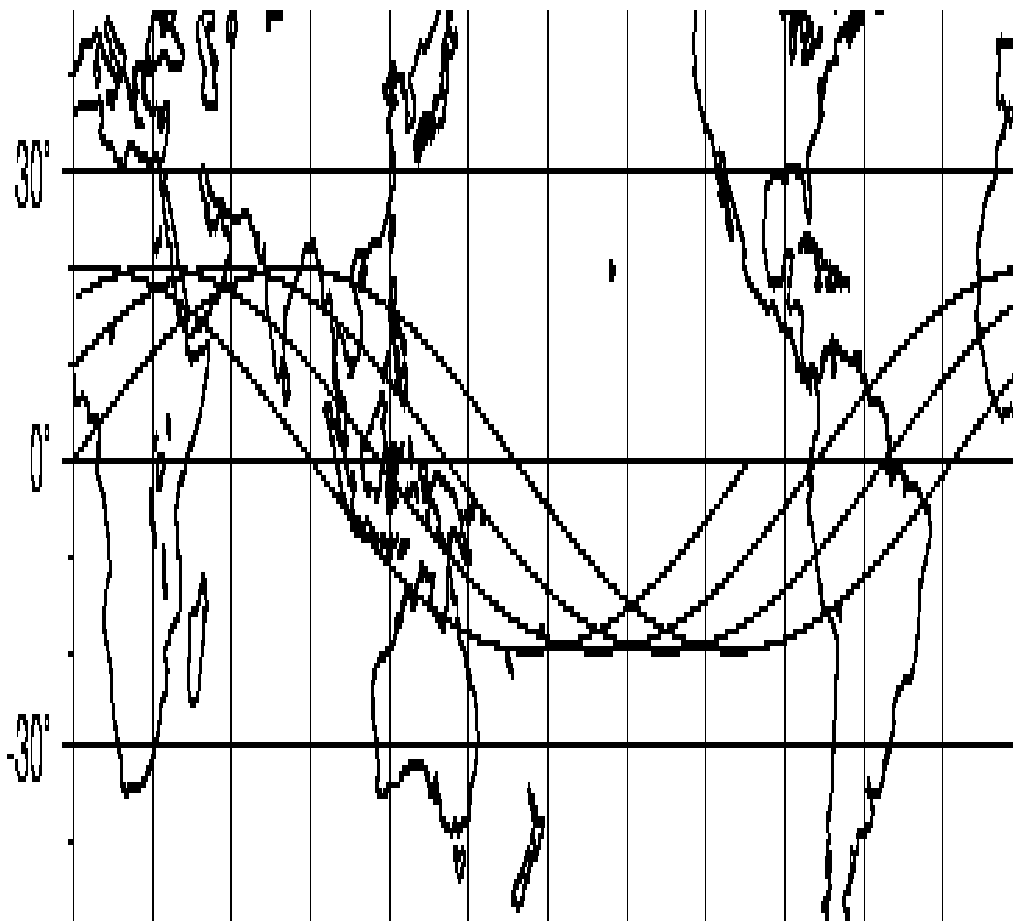


Figure 4: Four successive orbit tracks of the Megha-Tropiques Project.

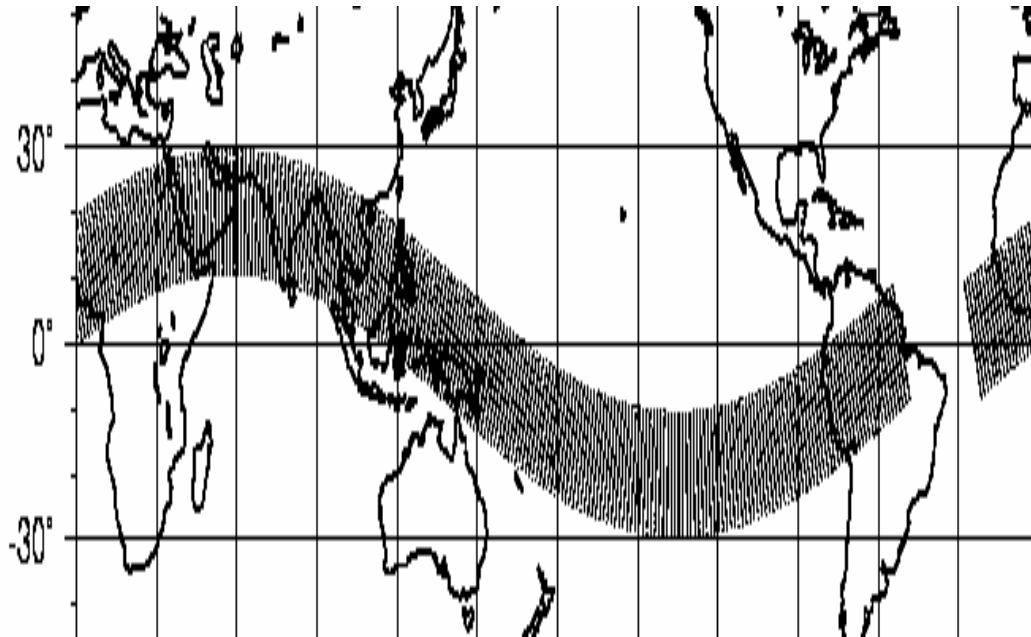


Figure 5: Swath of ScaRaB for one orbit of Megha-Tropiques.

0	1	2	3	4	5	6	7	8	9	10	11	12	13	14	15	16	17	18	19	20	21	22	23	0	1	2	3	4	5	6	7	8	9	10	11	12	13	14	15	16	17	18	19	20	21	22	23				
1	0	11	0	50	0	66	0	61	0	28	0	0	0	0	0	0	0	0	0	0	0	0	0	1	17	71	0	42	0	14	0	32	0	69	38	0	0	0	0	0	0	0	0	0	0	0	0	20			
2	0	14	0	51	0	63	61	0	28	0	0	0	0	0	0	0	0	0	0	0	0	0	0	2	0	73	0	41	0	14	31	0	71	0	35	0	0	0	0	0	0	0	0	0	0	0	0	23			
3	0	17	52	0	63	0	60	0	27	0	0	0	0	0	0	0	0	0	0	0	0	0	0	3	0	73	39	0	16	0	34	0	73	0	32	0	0	0	0	0	0	0	0	0	0	0	0	0	23		
4	20	0	54	0	65	0	59	24	0	0	0	0	0	0	0	0	0	0	0	0	0	0	0	4	74	0	39	0	16	0	37	73	0	31	0	0	0	0	0	0	0	0	0	0	0	0	0	0	26		
5	24	0	54	67	0	57	0	23	0	0	0	0	0	0	0	0	0	0	0	0	0	0	0	5	74	0	36	14	0	37	0	74	0	29	0	0	0	0	0	0	0	0	0	0	0	0	0	0	27		
6	0	57	0	70	0	57	0	23	0	0	0	0	0	0	0	0	0	0	0	0	0	0	0	6	0	35	0	16	0	36	0	74	26	0	0	0	0	0	0	0	0	0	0	0	0	0	0	0	28		
7	0	57	0	67	55	0	21	0	0	0	0	0	0	0	0	0	0	0	0	0	0	0	0	7	0	36	0	16	39	0	74	0	27	0	0	0	0	0	0	0	0	0	0	0	0	0	0	0	31		
8	58	0	64	0	52	0	17	0	0	0	0	0	0	0	0	0	0	0	0	0	0	0	0	8	36	0	16	0	39	0	74	0	24	0	0	0	0	0	0	0	0	0	0	0	0	0	0	0	33		
9	59	0	63	0	53	15	0	0	0	0	0	0	0	0	0	0	0	0	0	0	0	0	0	9	33	0	16	0	40	74	0	23	0	0	0	0	0	0	0	0	0	0	0	0	0	0	0	0	0	35	
10	60	64	0	51	0	13	0	0	0	0	0	0	0	0	0	0	0	0	0	0	0	0	0	10	32	16	0	42	0	74	0	21	0	0	0	0	0	0	0	0	0	0	0	0	0	0	0	0	38		
11	0	67	0	50	0	10	0	0	0	0	0	0	0	0	0	0	0	0	0	0	0	0	0	11	0	16	0	43	0	72	15	0	0	0	0	0	0	0	0	0	0	0	0	0	0	0	0	0	39		
12	0	70	49	0	8	0	0	0	0	0	0	0	0	0	0	0	0	0	0	0	0	0	0	12	0	16	44	0	71	0	12	0	0	0	0	0	0	0	0	0	0	0	0	0	0	0	0	0	43		
13	73	0	46	0	5	0	0	0	0	0	0	0	0	0	0	0	0	0	0	0	0	0	0	13	16	0	46	0	68	0	9	0	0	0	0	0	0	0	0	0	0	0	0	0	0	0	0	0	45		
14	68	0	45	2	0	0	0	0	0	0	0	0	0	0	0	0	0	0	0	0	0	0	0	14	18	0	47	67	0	5	0	0	0	0	0	0	0	0	0	0	0	0	0	0	0	0	0	0	49		
15	0	43	0	0	0	0	0	0	0	0	0	0	0	0	0	0	0	0	0	0	0	0	0	15	0	51	0	65	0	2	0	0	0	0	0	0	0	0	0	0	0	0	0	0	0	0	0	0	51		
16	0	43	0	0	0	0	0	0	0	0	0	0	0	0	0	0	0	0	0	0	0	0	0	16	0	51	0	63	0	0	0	0	0	0	0	0	0	0	0	0	0	0	0	0	0	0	0	0	51		
17	42	0	0	0	0	0	0	0	0	0	0	0	0	0	0	0	0	0	0	0	0	0	0	17	53	0	58	0	0	0	0	0	0	0	0	0	0	0	0	0	0	0	0	0	0	0	0	0	55		
18	40	0	0	0	0	0	0	0	0	0	0	0	0	0	0	0	0	0	0	0	0	0	0	18	54	0	58	0	0	0	0	0	0	0	0	0	0	0	0	0	0	0	0	0	0	0	0	0	57		
19	38	0	0	0	0	0	0	0	0	0	0	0	0	0	0	0	0	0	0	0	0	0	0	19	57	55	0	0	0	0	0	0	0	0	0	0	0	0	0	0	0	0	0	0	0	0	0	0	60		
20	0	0	0	0	0	0	0	0	0	0	0	0	0	0	0	0	0	0	0	0	0	0	0	20	0	52	0	0	0	0	0	0	0	0	0	0	0	0	0	0	0	0	0	0	0	0	0	0	64		
21	0	0	0	0	0	0	0	0	0	0	0	0	0	0	0	0	0	0	0	0	0	0	0	21	0	50	0	0	0	0	0	0	0	0	0	0	0	0	0	0	0	0	0	0	0	0	0	0	67		
22	0	0	0	0	0	0	0	0	0	0	0	0	0	0	0	0	0	0	0	0	0	0	0	22	48	0	0	0	0	0	0	0	0	0	0	0	0	0	0	0	0	0	0	0	0	0	0	0	67		
23	0	0	0	0	0	0	0	0	0	0	0	0	0	0	0	0	0	0	0	0	0	0	0	23	43	0	0	0	0	0	0	0	0	0	0	0	0	0	0	0	0	0	0	0	0	0	0	0	0	68	
24	0	0	0	0	0	0	0	0	0	0	0	0	0	0	0	0	0	0	0	0	0	0	0	24	26	0	0	0	0	0	0	0	0	0	0	0	0	0	0	0	0	0	0	0	0	0	0	0	0	70	
25	0	0	0	0	0	0	0	0	0	0	0	0	0	0	0	0	0	0	0	0	0	0	0	25	0	0	0	0	0	0	0	0	0	0	0	0	0	0	0	0	0	0	0	0	0	0	0	0	0	73	
26	0	0	0	0	0	0	0	0	0	0	0	0	0	0	0	0	0	0	0	0	0	0	0	26	0	0	0	0	0	0	0	0	0	0	0	0	0	0	0	0	0	0	0	0	0	0	0	0	0	73	
27	0	0	0	0	0	0	0	0	0	0	0	0	0	0	0	0	0	0	0	0	0	0	0	27	0	0	0	0	0	0	0	0	0	0	0	0	0	0	0	0	0	0	0	0	0	0	0	0	0	73	
28	0	0	0	0	0	0	0	0	0	0	0	0	0	0	0	0	0	0	0	0	0	0	0	28	0	0	0	0	0	0	0	0	0	0	0	0	0	0	0	0	0	0	0	0	0	0	0	0	0	74	
29	0	0	0	0	0	0	0	0	0	0	0	0	0	0	0	0	0	0	0	0	0	0	0	29	0	0	0	0	0	0	0	0	0	0	0	0	0	0	0	0	0	0	0	0	0	0	0	0	0	74	
30	0	0	0	0	0	0	0	0	0	0	0	0	0	0	0	0	0	0	0	0	0	0	0	30	0	0	0	0	0	0	0	0	0	0	0	0	0	0	0	0	0	0	0	0	0	0	0	0	0	74	
31	0	0	0	0	0	0	0	0	0	0	0	0	0	0	0	0	0	0	0	0	0	0	0	31	0	0	0	0	0	0	0	0	0	0	0	0	0	0	0	0	0	0	0	0	0	0	0	0	0	0	74

Table 4: The day-hour matrix of the simulated observations for a month in region near 20°N (upper left), 10°N (upper right), 20°S (lower left) and 10°S (lower right). The local time at the ascending node of the first orbit is 00:00. The number of observations falling in the 2.5° region is given in each hour box.

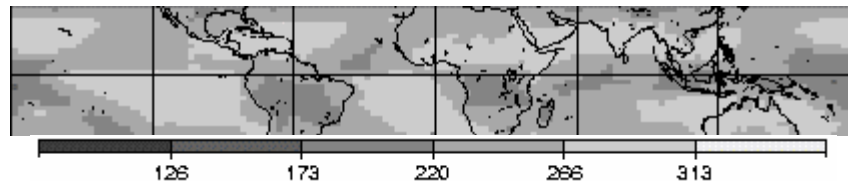


Figure 6: monthly means of the LW radiation (simulation for Megha -Tropiques) in Wm^{-2} .

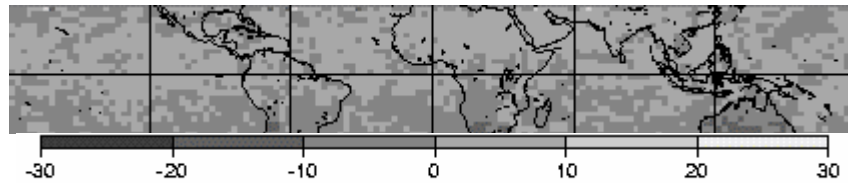


Figure 7: difference between LW simulation (figure 6) minus 'truth' in Wm^{-2} .

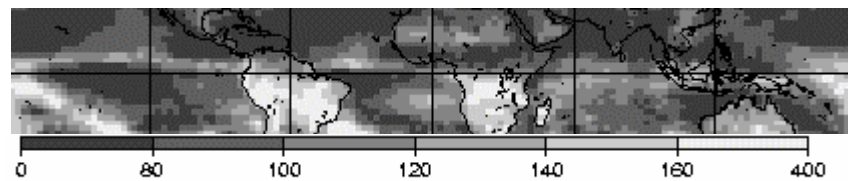


Figure 8: same as figure 6 but for SW reflected flux

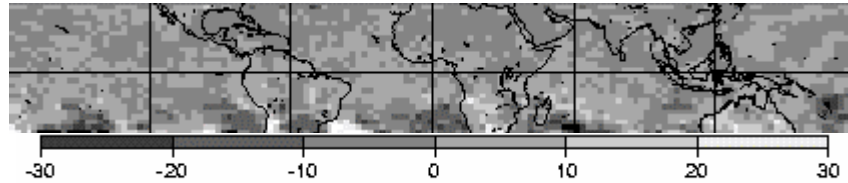


Figure 9: same as figure 7 but SW

The day-hour matrices (table 4) show that the temporal coverage is better at latitude 10° than at 20°. At 10°N, there are about 26 day-time observations, only 18 at 20°N. The same is observed at 10°S and 20°S but they are shifted to midday. The numbers in this table have been computed with the Local Time of the Ascending Node of the first orbit (LTAN1) at 00:00. Other LTAN1 give the same distribution but shifted in local time. The error maps (figure 7 and 9) correspond to LTAN1 of 12:00 (observation gaps on the South). Table 5 gives the errors (bias and standard deviation) for 3 cases of LTAN1: 00:00, 06:00 and 12:00. The highest errors are observed for LTAN1=12:00. This is because the southern latitudes, which receive the highest solar flux during December, are not observed at midday, contrary to the 00:00 case. However, table 5 shows that the errors are relatively low, near-zero bias, standard-deviation of 2.5 and 6.7 Wm⁻² respectively for LW and SW.

Local Time at the ascending node of the 1st orbit of the month.	LW		SW	
	bias	standard deviation	bias	standard deviation
00:00	0.2	2.2	0.4	5.5
06:00	-0.5	2.3	-0.8	6.3
12:00	-0.2	2.5	-0.5	6.7

Table 5: differences between simulation and 'truth' in Wm⁻² for 3 cases of LTAN1.

7 Conclusion

The ScaRaB data processing performs a triple integration (angular, regional and temporal) of the elementary raw radiances. Because many individual errors are statistically independent, the errors are reduced by the space and time averaging processes.

For the monthly means, simulations have shown that ScaRaB on Megha-Tropiques may give acceptable accuracy except near the edge (15-20°N, 15-20°S) of the observation zone due to periodical gaps in day-light observations of several days related to the orbit characteristics. Therefore such a mission should contribute to the time series of ERB estimates over Tropics. It can also be used in conjunction with CERES missions or other related missions.

However, the objective of Megha-Tropiques is focused on processes at a scale of 100 km and between a few hours to a few days, so that the error analysis on the regional instantaneous means must be pursued. Concerning the temporal coverage, table 4 (lower right) shows that the distribution is excellent (unique for SW) for selected periods.

8 References

- Bouffies-Cloch  S., J.P. Duvel, Ph. Dubuisson, and F.M. Br on 1998, 'Narrow-to-broad band conversion of Shortwave Radiances ' Estect Contract 11989/96/NL/CN
- Briand, V., C.J. Stubenrauch, W.B. Rossow, A. Walker, and R. Holz, 1997 : Scene identification for ScaRaB data: the ISCCP approach, in *Satellite Remote Sensing of Clouds and the Atmosphere* (ed. J.D. Haigh), *SPIE*, 242-252.
- Briand V., Stubenrauch C.J. and W.B. Rossow, 1999, 'Angular behaviour of shortwave reflectances as function of cloud scenes', Proceedings, ALPS99, WK2-P-27

- Brooks, D.R., E. H. Harrison, P. Minnis, J. T. Suttles, and R. Kandel, 1986: Development of Algorithms for Understanding the Temporal and Spatial Variability of the Earth's Radiation Balance, *Rev. Geophys.*, **24**, 2, 422-438.
- Capderou, M., 1998 Determination of the shortwave anisotropic function for clear-sky desert scenes from ScaRaB data. Comparison with models issued from other satellites. *Journal Of Applied Meteorology*, **37** 1398-1411
- Deschamps, P.-Y., F.-M. Bréon, M. Leroy, A. Podaire, A. Bricaud, J.-C. Buriez, and G. Sèze, 1994 : The POLDER Mission: Instrument Characteristics and Scientific Objectives. *IEEE Trans. Geoscience & Remote Sensing*, **32**, 598-615.
- Dlhopsky, R., A. Macke and R. Stuhlmann: 'A study of improved angular dependence models for radiation field measurements aboard future satellites', Final Report Esa Contract No, AO/1-2562/91/NL/SF, 1994.
- Doelling, D.R., L. Nguyen, W. L. Smith Jr., and P. Minnis, 1998 : Comparison of ARM GOES-derived broadband fluxes and albedos with broadband data from ARM-UAV, ScaRaB, and CERES. Proc. 8th ARM Science Team Meeting, (Tucson, AZ), March 23-27.
- Li, Z., and A. Trishchenko, 1999 : A study towards a better understanding of the relationship between visible and shortwave measurements. *J. Atm. Oc. Technol.*, **16**, 347-360
- Kandel R., M. Viollier, P. Raberanto, J.Ph. Duvel, L.A. Pakhomov, V.A. Golovko, A.P. Trishchenko, J. Mueller, E. Raschke, R. Stuhlmann, and the International ScaRaB Scientific Working Group (ISSWG), 1998 The ScaRaB Earth Radiation Budget Dataset, *Bulletin of the American Meteorological Society*, **79**, 765-783..
- Rossov et al., 1996: International Satellite Cloud Climatology Project (ISCCP). Documentation of New Cloud Datasets. WMO/TD
- Smith, G.L., R.N. Green, E. Raschke, L.M. Avis, J.T. Suttles, B.A. Wielicki, and R. Davies, 1986 : Inversion methods for satellite studies of the earth's radiation budget : development of algorithms for the ERBE mission. *Rev. Geophys.*, **24**, 407-421.
- Standfuss C., M. Viollier, P. Raberanto, J.P. Duvel, and R. Kandel 1998,' Diurnal Modelling for use in Earth radiation budget calculations ' Estect Contract 12173/97/NL/CN
- Stubenrauch, C., J.-P. Duvel, and R.S. Kandel, 1993 : Determination of longwave anisotropic emission factors from combined broad- and narrow-band radiance measurements, *J. Appl. Meteor.*, **32**, 848-856.
- Suttles, J.T., R.N. Green, P. Minnis, G.L. Smith, W.F. Staylor, B.A. Wielicki, I.J. Walker, D.F. Young, V.R. Taylor, and L.L. Stowe, 1988 : *Angular Radiation Models for the Earth-Atmosphere System*, **NASA RP-1184, Vol. 1 (SW radiation)**, 147 pp.
- Suttles, J.T., R.N. Green, G.L. Smith, B.A. Wielicki, I.J. Walker, V.R. Taylor, and L.L. Stowe, 1988 : *Angular Radiation Models for the Earth-Atmosphere System*, **NASA RP-1184, Vol. II (LW radiation)**, 87 pp.
- Trishchenko, A., and Z. Li, 1998 : Use of ScaRaB measurements for validating a GOES-based TOA radiation product. *J. Appl. Meteor.*, **37**, 591-605.
- Viollier, M., R. Kandel, and P. Raberanto, 1995 : Inversion and space-time averaging algorithms for ScaRaB (Scanner for Earth Radiation Budget) - Comparison with ERBE. *Annales Geophysicae*, **13**, 959-968.
- Wielicki, B.A., and R.N. Green, 1989 : Cloud identification for ERBE radiative flux retrieval. *J. Appl. Meteor.*, **28**, 1133-1146.